ADVANCED MATERIALS TECHNOLOGIES
www.advmattechnol.de

Extracellular Photovoltage Clamp Using Conducting Polymer-Modified Organic Photocapacitors

*Malin Silverå Ejneby, Ludovico Migliaccio, Mindaugas Gicevičius, Vedran Đerek, Marie Jakešová, Fredrik Elinder, and Eric Daniel Głowacki**

Optoelectronic control of physiological processes accounts for new possibilities ranging from fundamental research to treatment of disease. Among nongenetic light-driven approaches, organic semiconductor-based device platforms such as the organic electrolytic photocapacitor (OEPC) offer the possibility of localized and wireless stimulation with a minimal mechanical footprint. Optimization of efficiency hinges on increasing effective capacitive charge delivery. Herein, a simple strategy to significantly enhance the photostimulation performance of OEPC devices by employing coatings of the conducting polymer formulation poly(3,4-ethylenedioxythiophene):poly(styrene sulfonate), or PEDOT:PSS is reported. This modification increases the charge density of the stimulating photoelectrodes by a factor of 2–3 and simultaneously decreases the interfacial impedance. The electrophysiological effects of PEDOT:PSS-derivatized OEPCs on *Xenopus laevis* oocyte cells on membrane potential are measured and voltage-clamp techniques are used, finding an at-least twofold increase in capacitive coupling. The large electrolytic capacitance of PEDOT:PSS allows the OEPC to locally alter the extracellular voltage and keep it constant for long periods of time, effectively enabling a unique type of light-controlled membrane depolarization for measurements of ion channel opening. The finding that PEDOT:PSS-coated OEPCs can remain stable after a 50-day accelerated ageing test demonstrates that PEDOT:PSS modification can be applied for fabricating reliable and efficient optoelectronic stimulation devices.

1. Introduction

Neuromodulation devices artificially regulate neural processes by delivering controlled electrical stimulation.[1] The applications of these techniques are manifold, ranging from fundamental research to bioelectronic medical implants, which positively affect the lives of over a million patients worldwide.[2–4] In the clinical setting, electrical neural prostheses can modulate, restore, or bypass nerves, with the aim to restore sensory,[5] motor, or autonomic functions of the diseased or damaged nervous system.[4,6] There are several neuronal prostheses used on a large scale, such as cochlear implants, deep brain stimulators, and a variety of peripheral nerve stimulators for treating inflammatory disorders and chronic pain.[7] At present, the scope of new applications of bioelectronic medicine is expanding at a rapid pace.[8] Despite the diversity of application, all neuromodulation devices comprise a controllable power supply, pulse generator, electrodes in contact with the tissue, and interconnecting wires. The necessity of an implanted power supply and accompanying wiring represents a formidable obstacle, and has led many researchers to explore wireless technologies. Optical stimulation, leveraging highly mature and efficient solid-state light emitting technologies, has been one of the most promising avenues.[9–12] The tissue transparency window between 620–800 nm allows efficient and safe transmission of light through skin, tissue, and even bone.[13] Optoelectronic devices, which convert light impulses into electrical signals, offer the potential of localized, wireless, and minimally invasive stimulation of cells and tissues.[11,14] Optoelectronic

Dr. M. Silverå Ejneby, Dr. L. Migliaccio, M. Gicevičius, Dr. V. Đerek, M. Jakešová, Dr. E. D. Głowacki
Laboratory of Organic Electronics
Linköping University
Bredgatan 33, 602 21 Norrköping, Sweden
E-mail: eric.glowacki@liu.se

The ORCID identification number(s) for the author(s) of this article can be found under https://doi.org/10.1002/admt.201900860.

DOI: 10.1002/admt.201900860

Dr. M. Silverå Ejneby, Dr. L. Migliaccio, M. Gicevičius, Dr. V. Đerek, Dr. E. D. Głowacki
Wallenberg Centre for Molecular Medicine
Linköping University
SE-58185 Linköping, Sweden

Dr. M. Silverå Ejneby, Dr. F. Elinder
Department of Clinical and Experimental Medicine
Linköping University
SE-58185 Linköping, Sweden

M. Gicevičius
Faculty of Chemistry and Geosciences
Vilnius University
Naugarduko st. 24, LT-03225 Vilnius, Lithuania

Dr. E. D. Głowacki
Warsaw University of Technology
Faculty of Chemistry
00-664 Warsaw, Poland

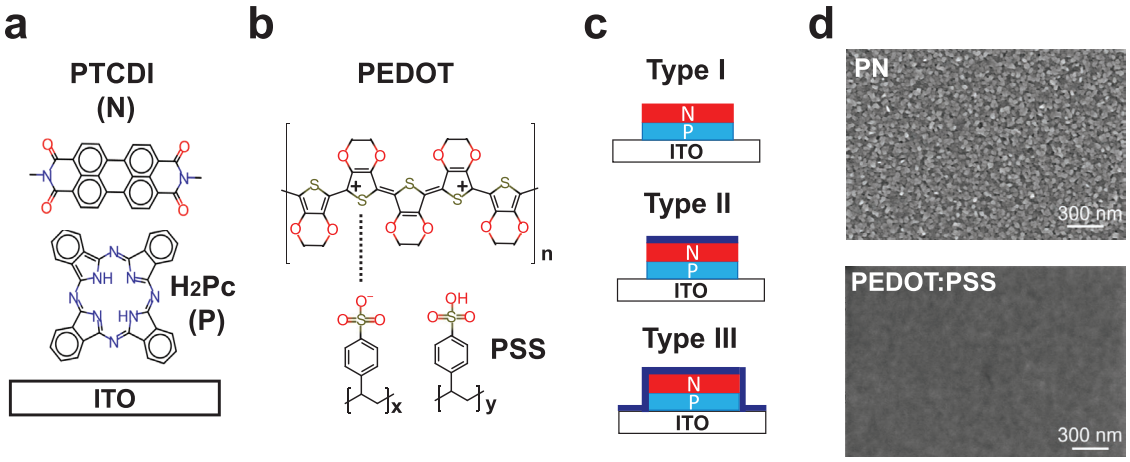

Figure 1. The OEPC device structure. a) Schematic drawing of the OEPC device, with the molecular structures of H_2Pc (light absorber and electron-donor, P) and PTCDI (electron-acceptor, N). PN layers consisting of 30 nm of each material are produced by vacuum sublimation through a shadow mask. b) Molecular structure of PEDOT:PSS. c) Schematic drawing of the three types of OEPCs devices compared in this work. The blue capping layer in Type II and III represents PEDOT:PSS coating. d) Scanning electron microscopy images of the PN surface before and after modification with PEDOT:PSS by spin-coating (5000 rpm = 55 nm thickness).

neuromodulation is of interest for biomedical applications, however it can also enable new in vitro research tools in electrophysiology[15] that are normally too difficult on account of complex wiring.

We have recently introduced the organic electrolytic photocapacitor (OEPC) as a simple thin-film device for cellular photostimulation.[16,17] It is fabricated from metal-free phthalocyanine (H_2Pc; p-type) and *N*,*N*′-dimethylperylene-3,4:9,10-tetracarboxylic diimide (PTCDI; n-type), deposited and patterned on top of a conductive back electrode. (**Figure 1**a,c; Type I device). The efficacy of OEPCs in neuromodulation was shown for cultured neurons and explanted retinal tissues where OEPCs stimulate direct action potentials in retinal ganglion cells of blind chick retinas.[16] More recently, the potential of OEPCs was validated by measuring large depolarizations of the membrane potential of *Xenopus laevis* oocytes, and accompanying opening of voltage-gated channels.[17] Advantages of the OEPC include that they are fabricated from biocompatible and nontoxic components, and are ultrathin, in the range of tens to hundreds of nanometers. The low thickness is possible because organic semiconductors can absorb deep red light efficiently. The *Xenopus laevis* oocyte model provides a robust test platform for new device concepts and for understanding the fundamentals of capacitive coupling behavior at the level of ion channel electrophysiology. Moreover, its round shape and 1 mm diameter provides a convenient model of a peripheral nerve. Peripheral nerves are one of the most important clinical neuromodulation targets.

To improve the efficiency of OEPCs, for both neuromodulation and extracellular stimulation of cells, two key parameters should be improved: electrolytic charge injection capacity and interfacial impedance. These two parameters apply generally to all stimulation electrode/microelectrode systems. To achieve these goals, in this work we turn to the conducting polymer poly(3,4-ethylenedioxthiophene):poly(styrene sulfonate) (Figure 1b, PEDOT:PSS). PEDOT:PSS belongs to the category of materials which are hybrid electronic and ionic conductors.[18] In aqueous environment, PEDOT:PSS swells with water, and has extremely high volumetric electrolytic capacitance.[19] PEDOT:PSS has recently emerged as one of the highest performance electrode materials for neuromodulation, excelling in the application of flexible multielectrode recording arrays.[20,21] The low impedance as well as stability PEDOT:PSS are key to its success.[22] PEDOT:PSS as a modification for stimulation electrodes has been explored less than for recording, however there are indications that high capacitance and low impedance could also cause PEDOT:PSS to be a good stimulation electrode material.[23] Herein we have explored PEDOT:PSS modification of the OEPC architecture and find that the performance of OEPCs is vastly enhanced in terms of capacitance and impedance. These conspire to increase the stimulation efficacy of OEPCs, which we benchmark using photoelectrochemical measurements, as well as single-cell electrophysiology in *Xenopus leavis* oocytes. The high capacitance afforded by PEDOT:PSS modification allows precise operation of the OEPC to act as an external capacitive voltage clamp electrode. This leads us to introduce a new concept of photovoltage clamp (without feedback circuit) for single-cell electrophysiology measurements—photovoltaic transductive extracellular potential (PVTEP) clamp.

2. Results and Discussion

2.1. Fabrication and Testing of PEDOT:PSS-Modified OEPCs

As a substrate for OEPC devices, we chose indium tin oxide (ITO) modified with octyltriethoxysilane as a hydrophobization layer which promotes good adhesion of the subsequent organic semiconducting layers. H_2Pc (30 nm, P) and PTCDI (30 nm, N) bilayers were processed by vacuum evaporation through a shadow mask (Figure 1a). This heterojunction, referred henceforth to as "PN", is responsible for photocharge generation in the OEPC. A commercial high-conductivity formulation of PEDOT:PSS (Figure 1b) could then be spin-coated

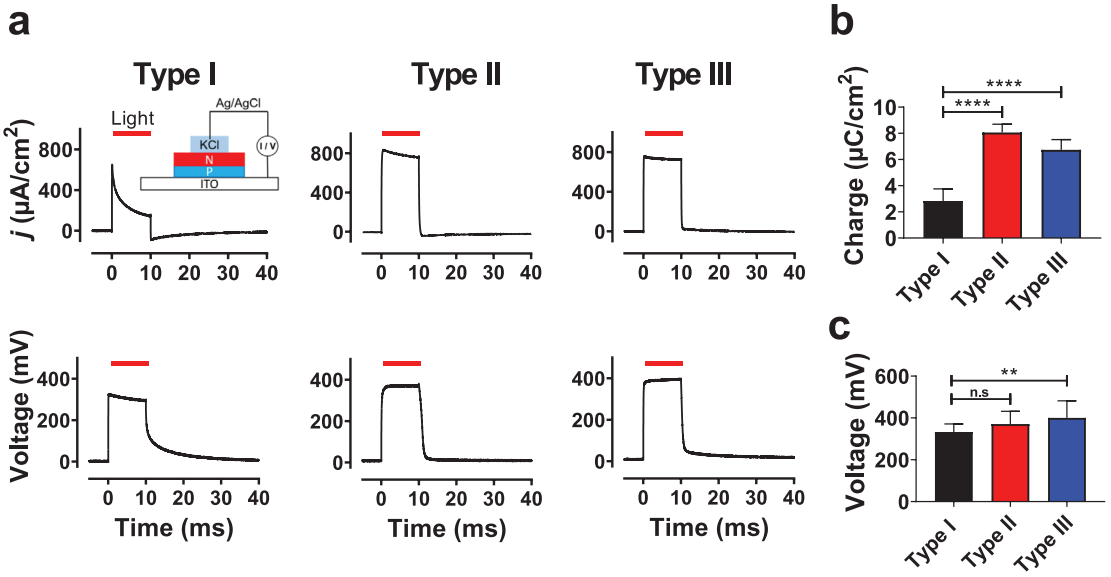

Figure 2. Electrophotoresponse (EPR) characteristics. a) EPR measurements of photocurrent density and photovoltage for Type I, II, and III devices (0.33 mW mm^{-2}). The inset shows a schematic of the EPR setup (see the Experimental Section). b) Photocharge density produced by a 10 ms light pulse. Charge density is at least two times higher for PEDOT:PSS-modified samples. **** = $p < 0.0001$. c) Maximal photovoltage. ** = $p < 0.01$. (b,c) Type I ($n = 18$), Type II ($n = 13$), Type III ($n = 18$).

on top of the device, followed by annealing. This resulted in a 55 ± 2 nm PEDOT:PSS layer, measured in the dry state. We compared three types of devices (Figure 1c): Type I – an unmodified OEPC as control, Type II – with PEDOT:PSS patterned only on top of the organic PN region, and Type III – with PEDOT:PSS covering the organic PN and surrounding ITO. To evaluate the coverage of the PEDOT:PSS on the PN layer and the morphology, we conducted scanning electron microscopy (SEM) imaging (Figure 1d). The PN layer alone has a distinctive nanocrystalline morphology, where crystallites which are tens of nanometers in size pack to form dense layers. The PEDOT:PSS, however, results in a conformal coating, which covers completely the underlying morphology, producing a smooth and defect-free coating. It should be noted that we attempted different spin speeds between 3000 and 6000 rpm, and found essentially the same performance of all these PEDOT:PSS-modified samples. Therefore, the whole study was conducted with 5000 rpm spin speed/55 nm thick PEDOT:PSS. Electropolymerization was also considered, but we found it too difficult to implement since the PN layers are photoconductors, and are highly insulating in the dark.

The performance of the OEPC devices was investigated by measuring the electrical photoresponse (EPR, schematized in **Figure 2**a inset). EPR gives information on the achievable photovoltage, current/charge density, and the charging/discharging dynamics of the device. EPR was performed at an irradiance of 0.33 mW mm^{-2} (Figure 2a). In EPR, voltage and current are measured between the back electrode (ITO) and an Ag/AgCl electrode immersed in 0.1 M KCl electrolyte, which is confined to a defined area above the device. For Type I devices, the photocharge density was 2.8 ± 0.2 μC cm^{-2} (using a 10 ms long light pulse), and the maximal photovoltage was 333 ± 10 mV ($n = 18$) (Figure 2b,c). The introduction of PEDOT:PSS into the structure of organic electrolytic photocapacitor device resulted in an increased photocharge density for Type II and III devices, and photovoltage for Type III devices (Figure 2b,c). The charge density and maximal photovoltage for Type II and III devices, respectively, were 8.1 ± 0.2 μC cm^{-2} and 371 ± 17 mV ($n = 13$), and 6.7 ± 0.2 μC cm^{-2} and 400 ± 19 mV ($n = 18$). The remarkable increase in current can be attributed to the electrolytic capacitance of PEDOT:PSS. The electrolytic capacitance of PEDOT:PSS is known to be outstanding, and due to its 3D hydrogel network, PEDOT:PSS has been referred to as a "volumetric capacitor". The increased interfacial capacitance afforded by PEDOT:PSS manifests itself also in the charging dynamics. A Type I device charging current peaks within tens of microseconds and then rapidly declines. For Type II and III devices, over a 10 ms light pulse, a persistent photocharging current is measured. Based on the transient charging behavior shown in Figure 2a, one can conclude that the PEDOT significantly increases (pseudo)capacitance as over 10 ms the charging current is essentially a plateau. An additional distinction is the lack of the anodic discharge peak apparent in Type I devices when illumination is turned off. This must be rationalized based on the actual electrochemical reactions taking place in this system: In a normal OEPC, negative charge carriers accumulate in the PTCDI layer at the interface with water, where corresponding cations create an electrolytic double layer. When light is turned off, these electrons in PTCDI recombine with holes in the PN junction, resulting in the anodic discharge peak. Due to slow recombination kinetics in the PN junction, as previously established, this anodic peak has slower kinetics than the cathodic rising current.[16] Upon modification of the OEPC with PEDOT:PSS, the behavior at the PTCDI/PEDOT interface is different. PEDOT:PSS is p-doped under normal conditions. During illumination, photogenerated electrons are presumably injected from PTCDI into the PEDOT layer, resulting in reduction of p-doped PEDOT to PEDOT$^{(0)}$. The capacity of

PEDOT:PSS to accommodate this reaction is indeed high, and over the course of the light pulse clearly current is injected at a nearly constant value. When light is turned off, however, there is no injection of charge carriers from the $PEDOT^{(0)}$ back into the PTCDI. For this reason, no anodic peak in EPR is visible. We hypothesize that the critical aspect in restoring and preserving the PEDOT:PSS function in such OEPCs is the presence of O_2, which will serve to oxidize the unstable $PEDOT^{(0)}$ back to $PEDOT^+$. It should further be noted that PEDOT:PSS on ITO itself does not show any photoeffects, as can be expected based on the fact that PEDOT:PSS is a degenerately doped semiconducting system.

Frequency-dependent electrochemical impedance response of illuminated organic electrolytic photocapacitor devices modified with PEDOT:PSS was registered in 0.1 M KCl solution at closed-circuit conditions versus a low-impedance, large-surface area Pt counterelectrode. In the dark, the PN layer is highly insulating, and PEDOT does not impact impedance. However, in illuminated devices, a clear difference is present. It is evident from electrochemical impedance spectra of PN and PN/PEDOT:PSS devices given in **Figure 3** that at low frequencies (1 Hz) conducting polymer-modified devices exhibit electrochemical impedance that is ten times lower than that of unmodified devices. These findings align well with studies of PEDOT:PSS-modifed recording and stimulation electrodes, where similar trends have been reported.[23–25] The increase in the interfacial capacitance and associated impedance drop have been ascribed to the volumetric capacitance effect of PEDOT:PSS formulations, recently elaborated by Proctor et al.[19]

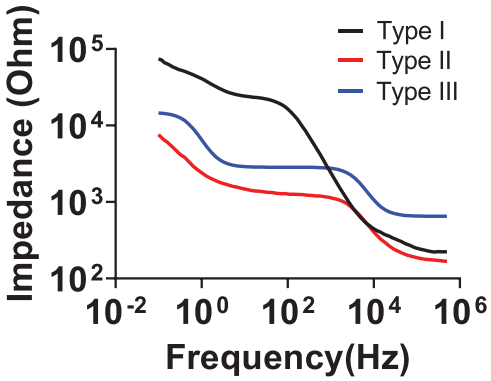

Figure 3. Electrochemical impedance of illuminated Type I, II, and III devices, measured under short-circuit conditions. These conditions mimic true operating conditions of the device. PEDOT:PSS leads to lowering of interfacial impedance in OEPC devices. Type III devices, which have PEDOT:PSS also on the ITO back contact, are measured to have higher impedance than Type II. This effect is due to the fact that the probe tip employed in the measurements to contact the device contacts ITO/PEDOT in the case of Type III, resulting in an additional in-series resistance.

2.2. Photoinduced Membrane Potential Modulation and Ion Channel Opening

2.2.1. Intracellular Transient Voltage (V_T) Changes

We have previously described *Xenopus laevis* oocytes as a useful model for studying stimulation with extracellular OEPCs. Briefly, an oocyte is placed on top of an OEPC device (13 mm ø), surrounded by electrolyte, and irradiation by 660 nm light pulses is delivered from below (**Figure 4**a). The stimulation performance of OEPCs can be characterized using voltage-follower and voltage-clamp techniques. This allows quantification of intracellular transient voltage changes (V_T) and validation of effective photostimulation by measuring the activation of ion channels. Since Type II and III devices have a higher charge density and higher capacitance, we hypothesized that these modified OEPCs will generate larger changes in the membrane potential of *Xenopus laevis* oocytes, and/or have longer-lasting effects when compared with Type I controls.

In the first set of measurements, we characterized OEPC effects on uninjected oocytes. These cells express very few endogenous ion channels and the effect of OEPC devices on membrane potential can then be evaluated without interference from ion channel opening/closing. Intracellular transient voltage changes (V_T), measured from Type I, II, and II devices, during a light pulse of 10 ms (6 mW mm^{-2}, 660 nm) are shown in Figure 4b. The potential difference is measured between the voltage electrode (at the upper intracellular region of the oocyte) and a distant reference electrode (Figure 4a). As described in our previous paper,[17] the measured V_T does not correspond, in magnitude or sign, to the membrane voltage, V_M, of the oocyte since the effect on the membrane voltage is dependent on the distance from the OEPC device, not the reference electrode. However, this cathodic transient voltage at the beginning of the light pulse (Figure 4b) is characteristic of OEPC devices, and as previously reported, this phase of the pulse leads to light-induced membrane depolarization. The depolarization is strongest at the interface of the bottom part of the oocyte where it contacts the surface of the OEPC.[17] An increased V_T correlates to an increased membrane depolarization, and the interplay of V_M and V_T are further discussed in Section 2.2.2. Both Type II and Type III devices increased the magnitude of the V_T at the maximal light intensity (6 mW mm^{-2}, 660 nm) from 116 ± 15 mV (Type I devices, $n = 4$), to 217 ± 10 mV (Type II devices, $n = 4$) and 280 ± 15 mV (Type III devices, $n = 5$). The maximum V_T as a function of light intensity for all three types of devices is plotted in Figure 4c. Type III devices overall performed better than Type II devices. At maximum light intensity, where one can assume that photogeneration is not a limiting factor, the magnitude of V_T increased by a factor of 2 for PEDOT:PSS-modified devices. This corresponds well with findings from EPR measurements, where charge density of PEDOT:PSS-modified devices was at least twice as high as Type I devices.

Aside from the obvious increasing V_T with PEDOT:PSS, the devices with PEDOT:PSS (Type II and Type III devices) also had longer-lasting effects on the membrane potential (Figure 4b,d,e). At the maximal light intensity (6 mW mm^{-2}, 660 nm), a Type I control device induces a V_T which decays within 3 ms. Type II devices decay over 20 ms, while Type III holds a transient potential over 200–300 ms (Figure 4d,e). When the light intensity was lowered (0.6 mW mm^{-2}) the V_T lasted even longer (Figure 4e). Lower light intensity corresponds to slower charging of the OEPC structure due to lower

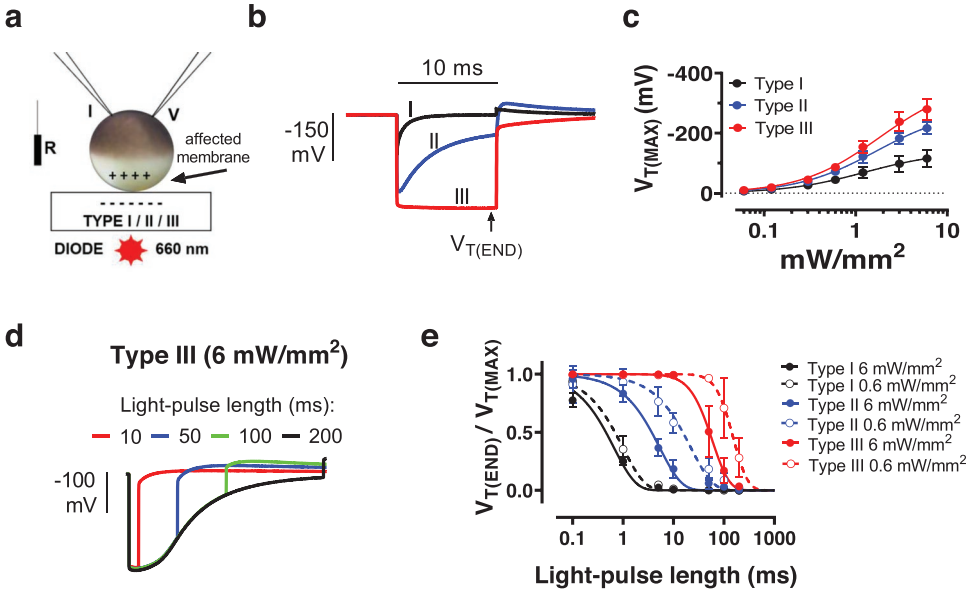

Figure 4. Intracellular transient voltage changes (V_T) in uninjected *Xenopus laevis* oocytes. a) Schematics of the OPEC/oocyte experiment. The oocyte is placed on top of an OEPC device, surrounded by electrolyte, and irradiation by 660 nm light pulses is delivered from below. The OEPC produces a transient perturbation in the potential, V_T, which is registered using a voltage-follower intracellular electrode (V) versus a reference electrode (R), placed in extracellular solution far away from the OEPC. b) V_T during a 10 ms light pulse (6 mW mm^{-2}, 660 nm) for Type I, II, and III devices. c) Maximal V_T at different light intensities. Mean ± SEM (n = 4–5). Maximal V_T and $I_{(1/2)}$ (Equation (1)) were −140 ± 12 mV and 1.3 ± 0.3 mW mm^{-2} (Type I), −281 ± 12 mV, and 1.7 ± 0.2 mW mm^{-2} (Type II), −372 ± 18 mV and 1.8 ± 0.3 mW mm^{-2} (Type III). d) Change in V_T for a Type III device using different light-pulse lengths. e) Relative V_T at the end of the light-pulse, at different light-pulse lengths, and light intensities (6 and 0.6 mW mm^{-2}). Data fitted with Equation (2). (Type I and II, n = 1, Type III 6 mW mm^{-2} n = 2.3, Type III 0.6 mW mm^{-2}, n = 3.8). Mean ± SEM, n = 4.

photogeneration of carriers. While the OEPC charges, there is a persistent displacement current in surrounding solution, resulting in a constant depolarizing transductive potential felt across the cell membrane. By dramatically increasing the capacitance of an OEPC using PEDOT:PSS, it is therefore possible to create a photoelectrode that can shift extracellular potential locally over long periods, thereby also extending the duration of effective membrane depolarization (Figure 4e). Taken together, the introduction of the conducting polymer PEDOT:PSS into the structure of the OEPC resulted in larger and long-lasting transient voltage effects on the membrane potential of *Xenopus laevis* oocytes.

2.2.2. Photovoltage Clamp Using an OEPC–Potassium Channel Opening

Given that Type III devices can afford a large and controllable perturbation of the membrane potential for relatively long periods of time (10+ ms), we tested if Type III devices could mimic the effect of a voltage clamp, in a way that you can shift the holding voltage by adjusting the light intensity. To test this, we first verified if Type III devices could depolarize the membrane sufficiently to trigger opening of the 3R Shaker K_V channel. We used the 3R mutant instead of wild-type since the 3R channel opens at more positive potentials from the resting potential. This allows us to use a higher light intensity range. The measured magnitude of V_T in 3R channel-expressing oocytes was 25% lower compared to uninjected oocytes, possibly due to the current leakage when ion channels open (**Figure 5**a). Nevertheless, the Type III devices had a long-lasting effect on the membrane potential (10+ ms), and there was no obvious effect on the light intensity dependence (Figure 5a). This confirms that channel-expressing oocytes respond similarly to the external OEPC as the uninjected oocytes. Knowing that the OEPC is delivering V_T in a similar way, we could move on to voltage-clamp tests to measure ion currents through the 3R K_V channels. During a voltage-clamp step protocol we applied 10 ms light pulses to the OEPC (0.3 mW mm^{-2}, 660 nm). Clearly, the Type III device depolarized the oocyte and increased the K^+ current (Figure 5b). The shift of the conductance versus voltage ($G(V)$) curve was −26 ± 3 mV (n = 4) and −62 ± 7 mV (n = 3), at a light-intensity of 0.3 and 0.6 mW mm^{-2}, respectively (Figure 5c,d). The device-induced $G(V)$ shift equaled around 65% of the V_T measured for uninjected oocytes discussed in Section 2.2.1 (Figure 5d).

Given this observation, we postulated that the light-intensity could be swept in order to produce a result analogous to a current–voltage curve. To test this, we conducted voltage-clamp measurements of oocytes expressing 3R Shaker K_V channels while holding the potential of the voltage clamp electrode constant (−100 mV) and sweeping the light intensity incident on the OEPC from 0.12 up to 3 mW mm^{-2}. K^+ currents measured from an oocyte during this photovoltage-clamp, compared with a conventional voltage-clamp protocol, are shown in Figure 5e. It is evident that a light-intensity sweep produced a result closely mimicking a conventional voltage-clamp protocol. However, the membrane potential around the oocyte during the "photovoltage-clamp" is likely not uniform, since a relatively larger membrane depolarization is expected at the OEPC/oocyte

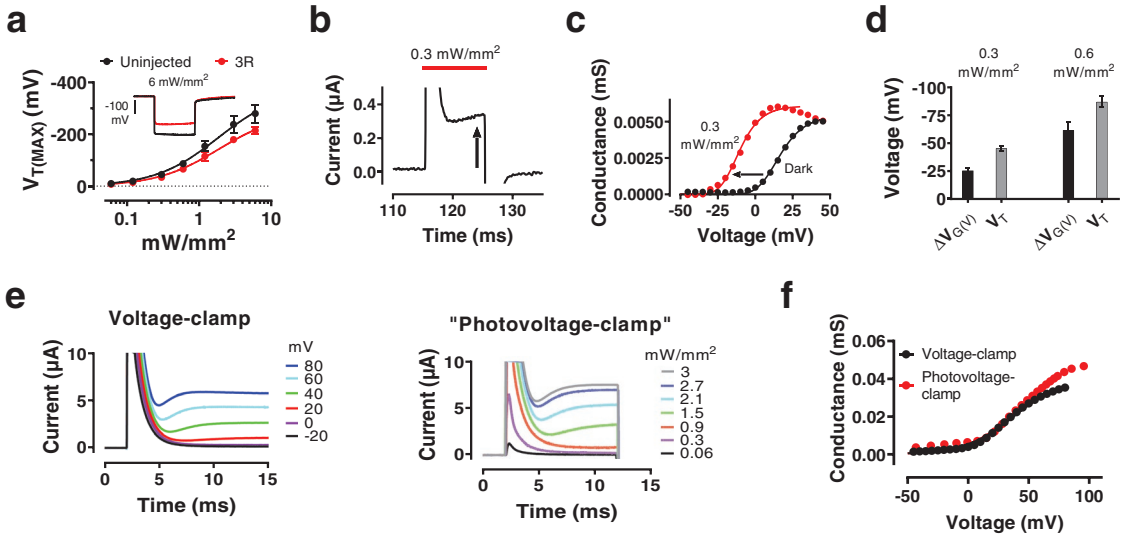

Figure 5. Type III devices used as an external photovoltage-clamp electrode. a) V_T values as a function of light intensity for uninjected oocytes (black) and oocytes expressing 3R K_V channels (red). The V_T in 3R channel-expressing oocytes is consistently 75% of the value of uninjected oocytes. V_T and $I_{(1/2)}$ (Equation (1)); –372 ± 18 and 1.8 ± 0.2 mW mm^{-2} (uninjected), –286 ± 11 mV and 1.9 ± 0.2 mW mm^{-2} (3R). Mean ± SEM, n = 4–5. Inset shows V_T traces during a 10 ms applied light pulse at 6 mW mm^{-2}. b) 3R Shaker K_V channel, K currents at –10 mV. Red line: light on for 10 ms (0.3 mW mm^{-2}, 660 nm). c) $G(V)$ curves in dark and light conditions. Shift = –25.4 mV. d) Device-induced $G(V)$ shift (3R Shaker K_V channel) and V_T measured from uninjected oocytes at corresponding light-intensity. e) K^+ currents from the same oocyte during a conventional voltage-clamp protocol, holding potential V_h = –100 mV (left), or with the photovoltage-clamp protocol (right), where V_h is left at a constant –100 mV and light intensity is swept. f) $G(V)$ curve for the 3R Shaker K_V channel using a conventional voltage-clamp protocol, and estimated $G(V)$ curve (using Equation (3), see the Experimental Section) for the photovoltage-clamp protocol.

interface.[17] A rough quantification of the average membrane potential for the whole oocyte, at a given light intensity, was calculated by estimating the average membrane depolarization to 65% of the measured V_T, from a holding potential of –100 mV, according to Equation (3) (see the Experimental Section). With this estimation a $G(V)$ curve could be plotted for the photovoltage-clamp protocol, together with a conventional voltage-clamp $G(V)$ curve (Figure 5f). There was no significant increase in the maximal conductance using the photovoltage clamp protocol estimation, and $\Delta V_{1/2}$ varied with ±20 mV for the tested oocytes, compared to conventional voltage clamp $G(V)$ curves.

2.3. Stability of OEPC Devices–Accelerated Aging Test

Long-term stability is important for a number of potential applications of OEPCs, and establishing in vitro robustness is a prerequisite for moving forward with potential chronic implant devices. We conducted aging tests on Type I, II, and III devices by storing them in electrolyte solution 0.1 KCl and periodically measuring EPR over the course of 50 days. One group of devices was kept in the dark at room temperature, while the second was heated at 40 °C and subjected to a light pulse stress of continuous charge/discharge cycles (a total of 8 million cycles over 50 days). The results for EPR currents and voltages are shown in **Figure 6**. It can be said that generally over time all devices give a decrease in performance parameters of voltage and current. Of Type I and Type II devices, not a single device failed, and all retain performance with current and voltage always more than half of the original value. Overall, Type II devices gave the best stability, superior to Type I controls. Type III

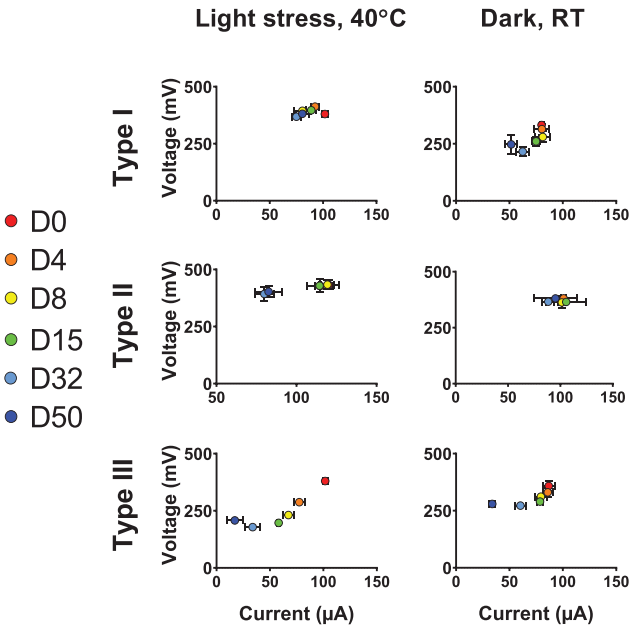

Figure 6. Stability of PEDOT:PSS-modified OEPC devices over 50 days in terms of EPR photovoltage (y-axes) and photocurrent (x-axes). Data on the left are from an accelerated ageing test in 0.1 M KCl, at 40 °C, under constant light-pulse stress (628 nm, 20 ms light pulses, 550 ms period = total of 8 million charge/discharge cycles over 50 days); data on right are for samples stored in 0.1 M KCl in the dark at room temperature. All devices show gradual drop in EPR performance in terms of photovoltage and current, though no devices show complete failure. The best performance stability was shown by Type II devices. Type III devices suffered from delamination of PEDOT:PSS from the ITO, clearly visible regardless of whether the samples were stressed or kept in dark at room temperature.

devices suffered from more substantial stability problems after two weeks. Interestingly, both light-stressed and devices kept in dark showed almost the same decline. Visual inspection as well as SEM investigation elucidates that the problem is delamination of the PEDOT:PSS from the ITO layer, and random redeposition of pieces of the delaminated film across the sample. PEDOT:PSS is also known, due to its locally acidic nature, to etch ITO. From this it can be concluded that PEDOT:PSS on the PN itself appears to be stable, and does not affect the device stability appreciably one way or the other. The adhesion and interface of PEDOT:PSS on ITO in such devices is a problematic point and in the future this combination should be avoided. It should also be stated that this test is primarily designed to establish stability under the stress of continuous operation in the form of charge–discharge cycles, nevertheless stability in an actual physiological environment may differ considerably due to adsorption of proteins or other factors. Future success of this device technology approach must hinge on stability assessment using in vitro or in vivo tests.

3. Conclusions

Here we report a strategy to significantly enhance the photostimulation performance OEPC devices by coating with PEDOT:PSS. The PEDOT:PSS modification enhances the performance of the OEPC device by increasing the charge density delivered by the electrode, due to increase in device capacitance, while simultaneously decreasing the impedance. Using *Xenopus laevis* oocytes at least a twofold increase in the stimulation efficacy of the PEDOT:PSS coated devices can be seen. The large capacitance of PEDOT:PSS allowed the OEPCs to depolarize the oocyte for a longer period of time (10+ ms). In turn, Type III devices could be used as a unique type of external, wireless, photovoltage-clamp, analogous to conventional voltage-clamp. It can mimic the effect of a voltage clamp, in a way that you can shift the holding voltage by adjusting the light intensity. As a general name for this concept, we would define it as PVTEP clamp. PVTEP can be used to wirelessly manipulate the membrane potential of adjacent cells for applications in electrophysiological research. An accompanying wireless readout of membrane currents would afford a fully wireless electrophysiology platform. PN PEDOT:PSS-coated OEPCs (Type II devices) can remain stable after a 50 days ageing test with 8 million charge/discharge cycles. These results suggest the elaboration of OEPCs for novel electrophysiology measurement tools, and also pave the way for OEPC use in wireless in vivo neuromodulation applications, like peripheral nerve stimulation. The current level of efficiency of OEPCs at the millimeter scale demonstrates that such photoelectrodes can operate on-par with similar-sized wired electrodes as are used for in vivo stimulation. Due to their size they do not operate at a highly localized cellular level such as some emerging nanoscale-based photostimulation approaches.[26] However, they operate at orders-of-magnitude lower light intensity than those cellular-level stimulation devices. Intensities of several mW mm^{-2} can easily and safely be transmitted through even ten to twenty mm of tissue or bone.[13] With continued optimization of photovoltage while keeping the electrolytic impedance low by employing methods like PEDOT:PSS modification, OEPC platforms can shrink further to also perform neurostimulation in a highly localized manner.

4. Experimental Section

Materials: Phthalocyanine H_2Pc (Alfa Aesar) and *N,N′*-dimethyl-3,4,9,10-perylenetetracarboxylic diimide, PTCDI (BASF) were purified by threefold temperature-gradient sublimation. For the preparation of the PEDOT:PSS films, 20 mL of aqueous dispersion (CLEVIOS PH 1000) was mixed with 1 wt% of dimethyl sulfoxide, and 2 wt% of 3-glycidoxypropyltrimethoxysilane (as a crosslinker), and the resulting dispersion was spin-coated. ITO-coated glass (Kintec) 15–20 Ohm sq^{-1} was used as a substrate. The ITO area under the organic layers of H_2Pc/PTCDI was modified with *n*-octyltriethoxysilane (Alfa Aesar).

Device Fabrication: 1 × 1 in. square ITO slides were cleaned by consecutive ultrasonication for 5 min in acetone, 2-propanol, and 2% Hellmanex III cleaning solution. The substrates were then rinsed with DI water and dried under a N_2 stream. The solvent cleaning was followed by 5 min O_2 plasma treatment (100 W) and coating the surface of the ITO with a monolayer of *n*-octyltriethoxysilane (OTS) by placing the samples in an OTS-vapor saturated chamber heated to 80 °C for 1 h. This improves the adhesion of organic PN layers to the ITO substrate. Excess of physioadsorbed OTS was removed by sonicating the samples in acetone for 5 min followed by rinsing twice with DI water and drying under N_2 stream. The organic pigment layers were formed by thermal evaporation deposition through a shadow mask at a base pressure of $<2 \times 10^{-6}$ Torr using a rate of 0.1–0.5 nm s^{-1}. 30 nm of P-type H_2Pc and 30 nm of N-type PTCDI were successively deposited resulting in the organic device (PN) of 60 nm thickness. The PN pixel was a 13 mm diameter circle in the center of the substrate. The modification of PN devices with PEDOT:PSS was performed by spin-coating at 5000 rpm at 1000 rpm s^{-1} acceleration for 60 s to obtain a well-adhered PEDOT:PSS coating (55 nm ± 2 nm, measured using scanning stylus profilometry). The films were subsequently baked at 140 °C for 1 h and were immersed in 0.1 M KCl to remove any excess low-molecular weight compounds as well as to allow the PEDOT:PSS to take up water and swell. All samples were then stored in 0.1 M KCl for 20 h before further use.

Electrophotoresponse EPR: Measurements of photovoltage and charging current of OEPC devices was performed according to previously described methods.[17] Briefly, the backside ITO of the OEPC was contacted with a probe electrode connected to the positive terminal of an oscilloscope. Meanwhile, the negative terminal was connected to an Ag/AgCl electrode in 0.1 M KCl electrolyte, making contact to the top of the organic layer of the OEPC device. An LED (630 nm) with intensity of 0.33 mW mm^{-2} was used.

Impedance Measurements: Impedance measurements of OEPCs were carried out in 0.1 M KCl in the frequency range 500 kHz to 0.1 Hz, using a BioLogic SP-300 Bipotentiostat. Two-electrode configuration was exploited for this characterization measuring in short-circuit condition at 0 V working electrode versus counterelectrode. Short-circuit condition was realized shorting the reference electrode (Ag/AgCl) to the counterelectrode (large surface area Pt electrode) and measuring at 0 V working electrode versus counterelectrode). Impedance was measured during illumination (630 nm, 33 mW cm^{-2}).

Electrophysiology: Oocyte (*Xenopus laevis*) preparation, storage, and RNA injection were done as described previously.[27,28] Animal experiments were approved by the local Animal Care and Use Committee at Linköping University. The 3R Shaker K_V channel, a modified wt Shaker K_V channel (M356R/A359R) with removed N-type inactivation, was used throughout the study.[29] The 3R Shaker K_V channel opens at more positive membrane voltages compared to wt Shaker *Kv* channel ($V_{1/2}$ = −21 mV (wt), $V_{1/2}$ = 25 mV 3R.[30] Therefore, higher light intensities could be used with the 3R. Electrophysiological measurements were done 1–4 days after RNA injection, or 1 day after oocyte harvesting for uninjected oocytes. The measurements were

performed with a GeneClamp 500B amplifier (Axon Instruments), pClamp 10 software (Molecular Devices) and a Digidata 1440A converter (Molecular Devices), as described previously.[17] For K currents, the amplifier leak compensation was used. The extracellular bath solution contained (in mM): 88 NaCl, 1 KCl, 15 HEPES, 0.4 $CaCl_2$, and 0.8 $MgCl_2$, pH was set to 7.4 with NaOH (all chemicals purchased from Sigma-Aldrich). All recordings were done in room temperature (20–23 °C). Briefly, the OEPC device was placed centrally above a light-emitting diode (660 nm, Thorlabs, 0.06–6 mW mm^{-2}, operated with a high-power LED Driver, DC2200 Thorlabs), in a petri dish filled with extracellular bath solution, and the oocyte in the middle, on top, of the OEPC PN pixel (see Figure 4a). All PEDOT:PSS-modified OEPC devices were stored in 0.1 M KCl for at least 2 days prior to measurements and washed with deionized water before being placed into the petri dish filled with extracellular bath solution.

Data Analysis: The transient voltage, V_T, is defined as the voltage change between resting membrane potential (dark conditions) and the intracellular potential during the light pulse. Potential is always relative to a distant reference electrode. To quantify the light-intensity dependence for the maximal V_T the following equation was used

$$V_{T(MAX)} = A/\left(1+I_{1/2}/I\right) \tag{1}$$

where A is amplitude of the curve, I is the light intensity and $I_{½}$ is the light intensity as which half-maximal response occurs.

For fitting the relative V_T change at the end of a light-pulse with increasing light-pulse length, a single-phase exponential decay curve was used

$$V_{T(END)}/V_{T(MAX)} = 1-\left(1-\exp\left(-t/\tau\right)\right)^n \tag{2}$$

where $V_{T(END)}/V_{T(MAX)}$ is the relative V_T at the end of a light-pulse, t is the light-pulse length, and τ is the time constant (in ms), and n is an exponent for better curve fitting due to the sigmoidal shape of the V_T decay for Type III devices. For Type I and II devices, on the other hand, n is set to 1.

When the photovoltage-clamp protocol was used, the holding potential was set to −100 mV, and the light-intensity was increased in 0.12 mW mm^{-2} steps up to 3 mW mm^{-2} (to avoid excessive depolarization and opening of endogenous ion channels). The average membrane potential of the whole oocyte, at each light intensity ($V_{m(light)}$) was then estimated accordingly

$$V_{m(light)} = f*\left(V_h-\left(A/\left(1+I_{(1/2)}/I\right)\right)\right) \tag{3}$$

where f is the relative ratio of membrane depolarization compared to the V_T measured for uninjected oocytes (estimated to 0.65, Figure 5c), V_h is the holding potential (set to −100 mV), A is the amplitude in the V_T versus light intensity curve (−371.7, Type III Figure 4c), I is the light intensity and $I_{(1/2)}$ is the light-intensity at which half-maximal response occurs (1.818, Type III Figure 4c).

The K conductance was calculated as

$$G_K(V) = I_K/(V_m - V_K) \tag{4}$$

where I_K is the steady-state current in dark, or in the end of a 10 ms light-pulse (the ionic current during a light-pulse was corrected for the light-induced capacitive current as described previously,[17] V_m the absolute membrane potential (or estimated membrane potential using the photovoltage-clamp protocol, Equation (3)), and V_K the reversal potential (set to −100 mV). The data were then fitted to a modified Boltzmann curve

$$G_K(V) = A/\left(1+\exp\left(\left(V_{1/2}-V\right)/s\right)\right)^n \tag{5}$$

where A is the amplitude of the curve, $V_{½}$ is the midpoint when $n = 1$, s is the slope, and n is an exponent for better curve fitting (set to 4).

Statistics: Average values are expressed as means ± SEM. When comparing device-induced responses a two-tailed unpaired t-test was used. A two-tailed one-sample t-test (mean value set to a hypothetical value of 1) was used to analyze changes in the maximal conductance. $P < 0.05$ was considered significant.

Acknowledgements

The authors gratefully acknowledge the financial support from the Knut and Alice Wallenberg Foundation within the framework of the Wallenberg Centre for Molecular Medicine at Linköping University, the Swedish Research Council (Vetenskapsrådet, 2018–04505), and the Swedish Foundation for Strategic Research (SSF).

Conflict of Interest

The authors declare no conflict of interest.

Keywords

cellular photostimulation, electrophysiology, organic bioelectronics, organic photovoltaics, PEDOT:PSS

Received: September 30, 2019
Revised: November 22, 2019
Published online: January 17, 2020

[1] *Neuromodulation* (Eds: E. S. Krames, P. H. Peckham, A. R. Rezai), Academic Press, London **2009**.
[2] I. Willner, E. Katz, *Bioelectronics*, Wiley-VCH, Weinheim, Germany **2005**.
[3] *Implantable Bioelectronics* (Ed: E. Katz), Wiley-VCH, Weinheim, Germany **2014**.
[4] *Handbook of Bioelectronics* (Eds: S. Carrara, K. Iniewski), Cambridge University Press, Cambridge **2015**.
[5] L. Ferlauto, M. Jole, I. Airaghi, N. Aurelia, L. Chenais, S. Charles, A. Gilliéron, P. Vagni, M. Bevilacqua, T. J. Wolfensberger, K. Sivula, D. Ghezzi, *Nat. Commun.* **2018**, *9*, 992.
[6] H. Acarón Ledesma, X. Li, J. L. Carvalho-de-Souza, W. Wei, F. Bezanilla, B. Tian, *Nat. Nanotechnol.* **2019**, *14*, 645.
[7] A. S. Caravaca, A. L. Gallina, L. Tarnawski, K. J. Tracey, V. A. Pavlov, Y. A. Levine, P. S. Olofsson, O. David, E. K. Ross, K. J. Otto, *Front. Neurosci.* **2019**, *13*, 877.
[8] K. Birmingham, V. Gradinaru, P. Anikeeva, W. M. Grill, V. Pikov, B. Mclaughlin, P. Pasricha, D. Weber, K. Ludwig, *Nat. Publ. Gr.* **2014**, *13*, 399.
[9] M. Scanziani, M. Häusser, *Nature* **2009**, *461*, 930.
[10] A. Canales, S. Park, A. Kilias, P. Anikeeva, *Acc. Chem. Res.* **2018**, *51*, 829.
[11] J. F. Zimmerman, B. Tian, *ACS Nano* **2018**, *12*, 4086.
[12] Y. Jiang, R. Parameswaran, X. Li, J. L. Carvalho-de-Souza, X. Gao, L. Meng, F. Bezanilla, G. M. G. Shepherd, B. Tian, *Nat. Protoc.* **2019**, *14*, 1339.
[13] S. L. Jacques, *Phys. Med. Biol.* **2013**, *58*, 5007.
[14] M. Sytnyk, M. Jakešová, M. Litviňuková, O. Mashkov, D. Kriegner, J. Stangl, J. Nebesářová, F. W. Fecher, W. Schöfberger, N. S. Sariciftci, R. Schindl, W. Heiss, E. D. Głowacki, *Nat. Commun.* **2017**, *8*, 91.
[15] Y. Jiang, B. Tian, *Nat. Rev. Mater.* **2018**, *3*, 473.

[16] D. Rand, M. Jakešová, G. Lubin, I. Vebraite, M. David-Pur, V. Đerek, T. Cramer, N. S. Sariciftci, Y. Hanein, E. D. Głowacki, *Adv. Mater.* **2018**, *30*, 1707292.
[17] M. Jakešová, M. S. Ejneby, V. Đerek, T. Schmidt, M. Gryszel, J. Brask, R. Schindl, D. T. Simon, M. Berggren, F. Elinder, E. D. Głowacki, *Sci. Adv.* **2019**, *5*, eaav5265.
[18] B. D. Paulsen, K. Tybrandt, E. Stavrinidou, J. Rivnay, *Nat. Mater.* **2019**, *19*, 13.
[19] C. M. Proctor, J. Rivnay, G. G. Malliaras, *J. Polym. Sci., Part B: Polym. Phys.* **2016**, *54*, 1433.
[20] M. Sessolo, D. Khodagholy, J. Rivnay, F. Maddalena, M. Gleyzes, E. Steidl, B. Buisson, G. G. Malliaras, *Adv. Mater.* **2013**, *25*, 2135.
[21] D. Khodagholy, J. N. Gelinas, Z. Zhao, M. Yeh, M. Long, J. D. Greenlee, W. Doyle, O. Devinsky, G. Buzsáki, *Sci. Adv.* **2016**, *2*, e1601027.
[22] S. Inal, J. Rivnay, A. O. Suiu, G. G. Malliaras, I. McCulloch, *Acc. Chem. Res.* **2018**, *51*, 1368.
[23] R. A. Green, P. B. Matteucci, R. T. Hassarati, B. Giraud, C. W. D. Dodds, S. Chen, P. J. Byrnes-Preston, G. J. Suaning, L. A. Poole-Warren, N. H. Lovell, *J. Neural Eng.* **2013**, *10*, 016009.
[24] D. Khodagholy, T. Doublet, M. Gurfinkel, P. Quilichini, E. Ismailova, P. Leleux, T. Herve, S. Sanaur, C. Bernard, G. G. Malliaras, *Adv. Mater.* **2011**, *23*, H268.
[25] A. Schander, T. Teßmann, S. Strokov, H. Stemmann, A. K. Kreiter, W. Lang, *Conf. Proc. of the IEEE Engineering in Medicine and Biology Society,* IEEE, Sweden **2016**, p. 6174.
[26] R. Parameswaran, J. L. Carvalho-De-Souza, Y. Jiang, M. J. Burke, J. F. Zimmerman, K. Koehler, A. W. Phillips, J. Yi, E. J. Adams, F. Bezanilla, B. Tian, *Nat. Nanotechnol.* **2018**, *13*, 260.
[27] S. I. Börjesson, T. Parkkari, S. Hammarström, F. Elinder, *Biophys. J.* **2010**, *98*, 396.
[28] N. E. Ottosson, X. Wu, A. Nolting, U. Karlsson, P.-E. Lund, K. Ruda, S. Svensson, P. Konradsson, F. Elinder, *Sci. Rep.* **2015**, *5*, 13278.
[29] N. E. Ottosson, S. I. Liin, F. Elinder, *J. Gen. Physiol.* **2014**, *143*, 173.
[30] M. Silverå-Ejneby, X. Wu, N. E. Ottosson, E. P. Münger, I. Lundström, P. Konradsson, F. Elinder, *J. Gen. Physiol.* **2018**, *150*, 731.